ELSEVIER

Contents lists available at ScienceDirect

# Earth and Planetary Science Letters

www.elsevier.com/locate/epsl



# Aragonite dissolution kinetics and calcite/aragonite ratios in sinking and suspended particles in the North Pacific



Sijia Dong <sup>a,\*</sup>, William M. Berelson <sup>a</sup>, Nick E. Rollins <sup>a</sup>, Adam V. Subhas <sup>b,c</sup>, John D. Naviaux <sup>b</sup>, Aaron J. Celestian <sup>d</sup>, Xuewu Liu <sup>e</sup>, Nitya Turaga <sup>a</sup>, Nathaniel J. Kemnitz <sup>a</sup>, Robert H. Byrne <sup>e</sup>, Jess F. Adkins <sup>b</sup>

- <sup>a</sup> University of Southern California, Los Angeles, CA, 90089, United States
- <sup>b</sup> California Institute of Technology, Pasadena, CA, 91125, United States
- <sup>c</sup> Woods Hole Oceanographic Institution, Woods Hole, MA, 02543, United States
- <sup>d</sup> Natural History Museum of Los Angeles County, Los Angeles, CA, 90007, United States
- <sup>e</sup> University of South Florida, St. Petersburg, FL, 33701, United States

#### ARTICLE INFO

# Article history: Received 8 November 2018 Received in revised form 8 March 2019 Accepted 10 March 2019 Available online 22 March 2019 Editor: D. Vance

Keywords: aragonite dissolution rate calcite/aragonite ratio North Pacific

#### ABSTRACT

The lack of consensus on CaCO3 dissolution rates and calcite to aragonite production and export ratios in the ocean poses a significant barrier for the construction of global carbon budgets. We present here a comparison of aragonite dissolution rates measured in the lab vs. in situ along a transect between Hawaii and Alaska using a <sup>13</sup>C labeling technique. Our results show a general agreement of aragonite dissolution rates in the lab versus in the field, and demonstrate that aragonite, like calcite, shows a non-linear response of dissolution rate as a function of saturation state  $(\Omega)$ . Total carbon fluxes along the N. Pacific transect in August 2017, as determined using sediment traps, account for 11~23 weight % of total mass fluxes in the upper 200 m, with a PIC (particulate inorganic carbon) /POC (particulate organic carbon) mole ratio of 0.2~0.6. A comparison of fluxes at depths of 100 m and 200 m indicates that 30~60% PIC dissolves between these depths with 20~70% attenuation in POC fluxes. The molar ratio of PIC to POC loss is 0.29. The simultaneous loss of PIC and POC in the upper 200 m potentially indicates PIC dissolution driven by organic matter respiration, or metazoan/zooplankton consumption. The calcite/aragonite ratio in trap material is significantly lower in the subtropical gyre than in the subarctic gyre. Aragonite fluxes vary from 0.07 to 0.38 mmol m<sup>-2</sup> day<sup>-1</sup> at 100 m, and 0.06 to 0.24 mmol m<sup>-2</sup> day<sup>-1</sup> at 200 m along the North Pacific transect, with no specific trend over latitude. The identification of suspended PIC mineral phases by Raman spectroscopy shows the presence of aragonite below 3000 m in the subtropical gyre, but none in the subpolar gyre. These multiple lines of evidence suggest that predictions based on a strictly thermodynamic view of aragonite dissolution, combined with measured aragonite fluxes, underestimate observed alkalinity excess and measured PIC attenuation in sinking particles. Our measured aragonite flux combined with our inorganic dissolution rate only account for 9% and 0.2% of the excess alkalinity observed in the North Pacific (Feely et al., 2004), assuming aragonite sinking rates of 1 m day<sup>-1</sup> and 100 m day<sup>-1</sup>, respectively. However, respiration-driven dissolution or metazoan/zooplankton consumption, indicated by the simultaneous attenuation of PIC and POC in sediment traps, is able to generate the magnitude of dissolution suggested by observed excess alkalinity.

© 2019 Elsevier B.V. All rights reserved.

#### 1. Introduction

The size of the total carbon inventory and its distribution within the ocean has a major influence on the partitioning of carbon between the ocean and the atmosphere, the net uptake of

\* Corresponding author.

E-mail address: sijiadon@usc.edu (S. Dong).

anthropogenic CO<sub>2</sub> by the ocean, and thus global climate. Calcium carbonate dissolution is a key process in ocean carbon cycling and many of the uncertainties in diagnostic and prognostic marine carbon cycle models arise from an imperfect understanding of the correct formulation for the dissolution of CaCO<sub>3</sub> (Iglesias-Rodriguez et al., 2002). An outstanding problem is the relative roles of water column and sedimentary dissolution in setting the ultimate burial rates of CaCO<sub>3</sub> in the ocean.

Shallow-depth water column CaCO3 dissolution where calcite is supersaturated has been documented by several independent studies (Anderson and Sarmiento, 1994; Lohmann, 1995; Schiebel, 2002), and the dissolution of more soluble forms of CaCO3 including aragonite and high-Mg calcites has been suggested as one possible mechanism for the observed alkalinity enrichments (Byrne et al., 1984; Iglesias-Rodriguez et al., 2002; Honjo et al., 2008). Specifically, the export of pteropod shells (aragonite) to the mesopelagic water column offers investigators a tenable source for elevated alkalinity in the upper mesopelagic zone (Betzer et al., 1984; Byrne et al., 1984; Feely et al., 2004). However, compared to the numerous studies addressing the dissolution kinetics of calcite in seawater (Honjo and Erez, 1978; Keir, 1980; Gehlen et al., 2005; Subhas et al., 2015; Dong et al., 2018; Naviaux et al., 2019), only a modest number of investigations focused on the dissolution behavior of aragonite (Milliman, 1975; Honjo and Erez, 1978; Morse et al., 1979; Keir, 1980; Acker et al., 1987). As a result, studies of the marine aragonite cycle are limited by the lack of available information on aragonite dissolution kinetics (Gangstø et al., 2008), as well as well-quantified aragonite production and export rates (Honjo et al., 2008).

Most kinetics studies of the dissolution behavior of CaCO3 in seawater have expressed the dependence of dissolution rate on seawater saturation state through the empirical equation Rate =  $k(1-\Omega)^n$ , where k is the rate constant, and n is the pseudo reaction order. Discontinuities in the function of calcite dissolution rate vs. under-saturation in seawater, defined as  $\Omega_{critical}$ , have been documented in recent studies (Subhas et al., 2017; Dong et al., 2018; Naviaux et al., 2019). These authors assert that the discontinuities are related to changes in dissolution mechanisms, transforming from step retreat to defect-assisted dissolution, and to the homogeneous spreading of etch pits, as seawater gets more undersaturated. Reported dissolution rates for aragonite in seawater are different by as much as 4 orders of magnitude, depending on the experimental conditions (lab vs. field) and sample type (synthetic aragonite vs. pteropods), making the estimate of aragonite dissolution fluxes in the ocean highly uncertain.

Pteropods are the major pelagic species in the ocean that make their shells out of aragonite. These relatively large (1~20 mm) biogenic particles sink after death and may dissolve while sinking, providing alkalinity that can be supplied back to the surface ocean via upwelling and diapycnal mixing. Among the previous studies that quantified the biogenic inorganic carbon export fluxes (Honjo et al., 1982; Berelson, 2001; Klaas and Archer, 2002; Balch et al., 2005; Berelson et al., 2007; Boyd and Trull, 2007; Bishop and Wood, 2008), estimates of aragonite production and fluxes are scarce, and span a range from 1 to 50% of the total global CaCO3 flux (Berger, 1978; Berner and Honjo, 1981; Fabry, 1989; Fabry and Deuser, 1991; Hong and Chen, 2002; Mohan et al., 2006). Because of the significant difference between the solubility and dissolution rates of calcite and aragonite, it is impossible to quantify CaCO<sub>3</sub> dissolution from the sinking biogenic fluxes without knowing the calcite/aragonite ratio of the sinking

We present here a high-resolution map of aragonite saturation in a North Pacific transect (Fig. 1), and aragonite dissolution rate measurements from both laboratory experiments and the North Pacific transect. We also show calcite/aragonite ratios in sinking and suspended particles along the transect. These data are used to address whether aragonite dissolution in the water column can account for the observed excess alkalinity reported for North Pacific Intermediate Water (600 m to 900 m). We also investigate dissolution that is driven by organic matter respiration or metazoan/zooplankton grazing by analyzing the attenuation of sinking PIC and POC through the water column. Our new constraints on

the export fluxes of calcite and aragonite highlight the role of aragonite dissolution in ocean carbon and alkalinity budgets.

#### 2. Methods

#### 2.1. Labeled aragonite for dissolution experiments

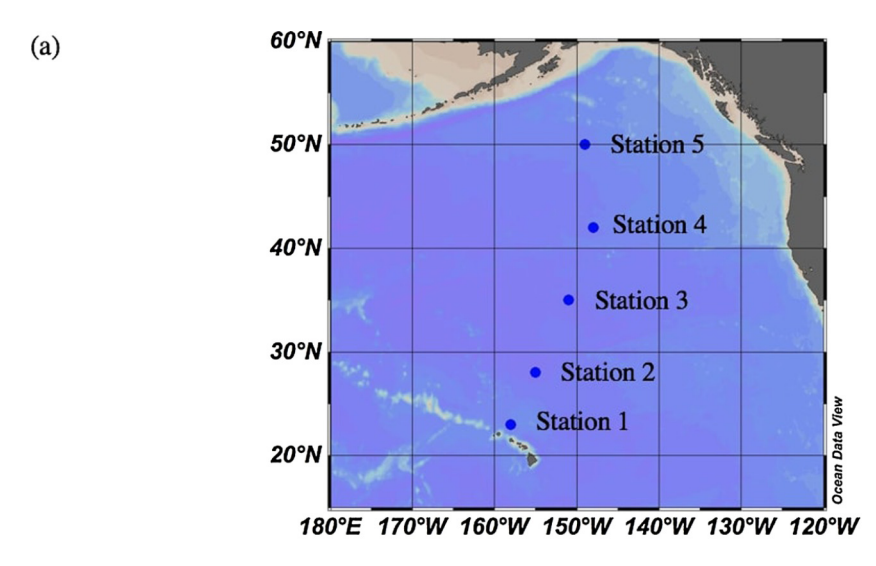
<sup>13</sup>C labeled aragonite used for all the dissolution experiments was synthesized in our laboratory using a gel-diffusion method first described by Nickl and Henisch (1969). A 120 mL glass Ushaped tube was filled with 30 mL hydrous gel (0.17 M sodium metasilicate, adjusted to pH 8), separating ~40 mL reservoirs of Na<sub>2</sub><sup>13</sup>CO<sub>3</sub> (0.20 M) in one arm of the tube, and 40 mL CaCl<sub>2</sub>  $(0.10 \text{ M}) + \text{MgCl}_2 (0.50 \text{ M})$  in the other arm of the tube. The ends of the tube were sealed using Parafilm and rubber stoppers. Nucleation of aragonite crystals was limited by diffusion in the hydrous gel and the gel pore spacing, allowing for slow growth of large crystals. Grains were harvested after 3-6 months of reaction time by pouring off the spent reservoir solutions followed by physical break-up, sonication, and decantation of the less dense gel matrix from the aragonite grains. Grains were then triply washed in Milli-Q water. The mineral grains were wet-sieved to a grain size of 250-495 µm and dried at 60 °C overnight.

Mineralogy was confirmed with XRD and Raman spectroscopy. SEM imagery was obtained using a Hitachi TM-1000 environmental SEM (Fig. S1).  $\delta^{13} C$  of the synthetic aragonite was determined using a Picarro Cavity Ring-Down Spectroscopy (G2131-i) by sequentially diluting small aliquots of materials (0.2~0.8 mg) into natural abundance optical calcite and measuring the isotope composition of the mixtures. The degree of  $^{13} C$  isotope labeling of the synthetic aragonite was determined to be 100  $\pm$  5%. Specific surface area was measured using Kr adsorption isotherms, fitting the curves following the BET method. BET surface area was determined to be 2.46  $\pm$  0.05 m²/g. Kr has been demonstrated to give accurate surface areas down to 0.05 m² total area (Subhas et al., 2015). Therefore, the specific surface area determined for the U-tube  $^{13} C$  aragonite, with a sample mass of 0.54 g and a total area of 1.3 m², was considered well-constrained.

## 2.2. Lab and field dissolution experiments

Lab dissolution experiments were conducted following the method reported in earlier publications of our group (Subhas et al., 2015). Briefly, <sup>13</sup>C labeled aragonite was dissolved in acidified Dickson standard reference seawater (https://www.nodc.noaa. gov/ocads/oceans/Dickson\_CRM/batches.html), and  $\delta^{13}$ C of seawater DIC was traced over time to establish dissolution rates. DIC and alkalinity were measured to determine  $\Omega$  before and after each 3 to 5-days experiment. Dissolution experiments were conducted on a shaker table at 60 rpm, at ambient room temperature (21 °C) and a temperature most representative of in situ ocean temperature at 200~2000 m depth (5°C). Because the mass of solid was small (1 mg) compared to seawater (300 g),  $\Omega$  never changed by more than 0.03 during an experiment. The errors in alkalinity and DIC were propagated to  $\Omega$  by a Monte Carlo approach (Subhas et al., 2015). The errors in dissolution rates were calculated based on the goodness of fits in  $\delta^{13}$ C-time correlation using the LINEST function in Microsoft Excel. The stoichiometric solubility product of aragonite  $(K_{sp}^*)$  used to calculate  $\Omega$  was reported by Mucci (1983).

Field dissolution rates were measured at 4 stations along a North Pacific transect between Honolulu, Hawaii and Seward, Alaska (Fig. 1) in August, 2017. The cruise crossed from the subtropical gyre into the subarctic gyre, passing through the transition zone – a large-scale frontal system between the two gyres that has high productivity and particle export. Dissolution experiments were conducted in custom-built Niskin Incubators. These devices



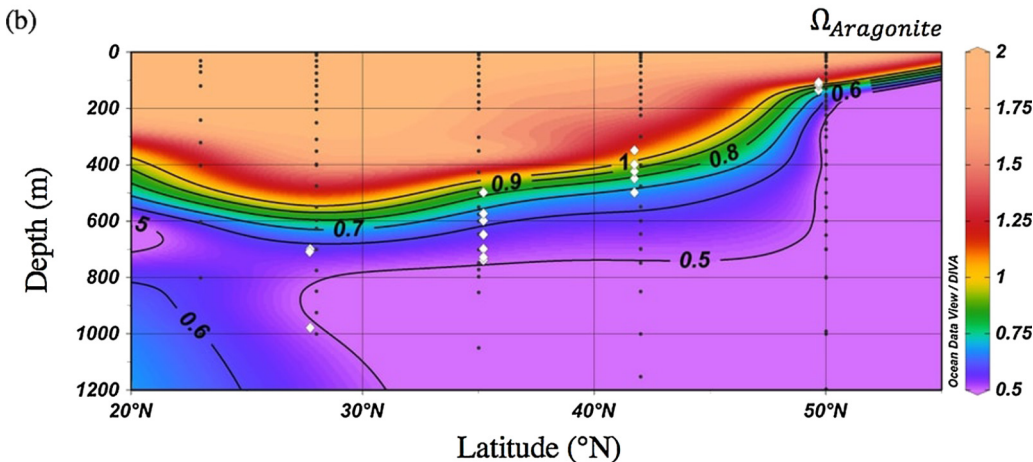


Fig. 1. (a) A map of the Northeast Pacific Ocean and station locations for the CDisK-IV Cruise (August, 2017); (b)  $\Omega_{Aragonite}$  in the upper 1200 m along the transect. White diamonds are locations where in situ aragonite dissolution experiments were conducted in Niskin Incubators (Station 2 to 5). There was an additional deployment at 2020 m, Station 2, ( $\Omega_{Aragonite} = 0.57$ ) that is not shown in Fig. 1b.  $\Omega_{Aragonite}$  in Fig. 1b is calculated based on alkalinity and pH measurements of CDisK-IV CTD cast, and is slightly different from  $\Omega_{Aragonite}$  data from GLODAP v2 ODV collection. This discrepancy will be discussed in detail in a forthcoming paper of our group.

were modified General Oceanics 1.7 L Niskins. Approximately 1 mg of <sup>13</sup>C labeled aragonite powders were placed in a membrane bag of 8 µm pore size (Whatman Nuclepore Track-Etched Membranes, WHA111114), and inserted into a closed "toaster" chamber that was connected to the Niskin bottle through MasterFlex tubing (Tygon Fuel & Lubricant Tubing, 06401-82 and 06401-17). A Seabird SBE 5T/5P Submersible Pump was connected to each Niskin Incubator to generate circulation inside the reactor so that sufficient mixing was provided as water continuously passed through the "toaster" and through the Niskin. This occurred while Niskins traveled down the water column to the target depth. Messengers then triggered Niskin closure and carbonate dissolution proceeded at in situ conditions until the Niskins were recovered and sampled. Discrete samples were taken from the CTD (conductivity, temperature, and depth) cast and incubator cast.  $\delta^{13}C$  of DIC obtained from the CTD cast and from the incubator cast was compared to determine dissolution rates. The uncertainty of dissolution rates depends on the standard deviation of the replicate samples. pH (total scale) and alkalinity were measured by the group in Byrne lab, University of South Florida to determine  $\Omega$  in the water column. The determination of  $\Omega$  by the DIC-alkalinity pair (lab method), and the pH-alkalinity pair (field method) agreed with each other (Table S1).

## 2.3. Sinking flux measurements with sediment traps

An array of surface-tethered sediment traps was deployed on a single line; one at 100 m and the other at 200 m depth at the 5 stations in the North Pacific transect. Traps were deployed as free-floating arrays for 52 to 78 h. The traps were polycarbonate particle interceptor tubes (PIT) that were 70 cm long, 10 cm diameter (12 tubes per trap) with funnels inserted to guide particles into a Falcon tube attached to the end of the funnel. Falcon tubes were pre-filled with HgCl2 poison in brine solutions to inhibit diffusive loss of poison during deployment. The poison-brine solution was made from seawater collected at 150 m with NaCl added to increase the salinity by  $\sim$ 5, and sodium borate was added to increase alkalinity by  ${\sim}2000~\mu\text{M}$  (US JGOFS protocol). Samples from 6 arbitrarily-chosen tubes among the 12 tubes at the same depth were combined and 'swimmers' were manually picked out. The samples were then filtered onto a pre-weighed glass fiber filter (Whatman glass microfiber filters, Grade GF/F, 1825-047) and, after being returned to the lab, were reweighed to calculate sinking mass flux. The solid materials on the filters were then collected and analyzed with XRD for mineralogy, and with the Picarro for PIC and total C. The uncertainty associated with the sediment trap method was evaluated by comparing the duplicate samples at 100 m, Station 4.

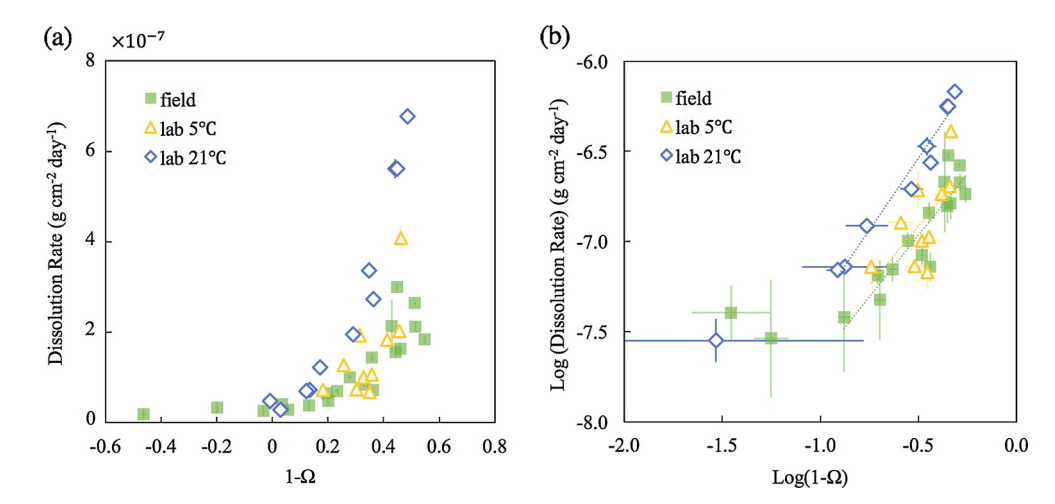


Fig. 2. Aragonite dissolution rates measured in the field along the North Pacific transect (2~7°C), and in the lab (5°C and 21°C). (a) Specific dissolution rates (g cm<sup>-2</sup> day<sup>-1</sup>) vs. (1 – Ω); (b) log-log scale of specific dissolution rates (g cm<sup>-2</sup> day<sup>-1</sup>) vs. (1 – Ω). The reaction orders (slopes of the fitting lines) of field, lab 5°C, lab 21°C rate laws at  $\Omega = 0.45 \sim 0.87$  are 1.37  $\pm$  0.18, 1.33  $\pm$  0.56, and 1.59  $\pm$  0.12 respectively. At  $\Omega = 0.9 \sim 1$  [log(1 – Ω) < -1.0], reaction order *n* is smaller than at lower Ω. The transition between the two reaction orders ( $\Omega_{critical}$ ) occurs at  $\Omega_{critical} \sim 0.9$ .

Calcite/aragonite ratios were analyzed based on the relative peak intensity of the strongest calcite (104) and aragonite (111) peak in XRD. Standards of 6 different ratios of calcite-aragonite mixtures were measured to generate a calibration curve of peak intensity ratio versus concentration (Fig. S2).

# 2.4. Suspended particle concentration measurements with in situ pumps

Suspended particles were captured on an Advantec GC-50 Glass Fiber Filter (LOT No. 70207718, pore size 0.5 µm, diameter = 142 mm) through filtration of a dual-flowpath in situ pump (McLane WTS-6-1-142LVUP). At targeted depths, approximately 1400 L of seawater were pumped through the filter. Upon recovery, the filter was sub-sampled into smaller circles by using two different sized punches. These sub-samples were used for PIC, total C and calcite/aragonite ratio measurements. Circles of 26 mm diameter and 6.75 mm diameter were taken for Picarro measurements of PIC and total C, respectively. PIC and total C were determined by measuring the amount of CO2 released after acid treatment and combustion. A circle of 26 mm diameter was analyzed for mineral composition on a Horiba ExploRa+ dispersive Raman microscope after being treated with 50% bleach to remove organic matter which otherwise would inhibit the Raman spectroscopy laser (532 nm). A 1 gL<sup>-1</sup> sodium borate buffer was added to the bleach to preclude potential CaCO3 dissolution during the bleaching process. The Raman analysis was programmed as an 8 mm × 8 mm scan of each bleached filter, and a map of calcite and aragonite distribution was generated. Calcite/aragonite ratios were calculated by ImageJ based on two different counting methods. First, total counts for each mineral were identified by the software. The minimum carbonate size detected (30  $\times$ 30 µm) was limited by the size of a single image pixel. Second, the total area occupied by each mineral was analyzed. The two methods were in general agreement (Fig. S3), except for filters that included a single large calcite or aragonite fragment. Mineral percentages calculated by total area took into account the size differences of particles. However, random inclusion of a single large particle could potentially bias the calcite/aragonite ratio. Therefore, the analysis of suspended calcite/aragonite percentages and concentrations in this paper was based on the counts of the two minerals.

#### 3. Results

#### 3.1. Aragonite dissolution rates

Both aragonite lab and field dissolution rates show a non-linear relationship with seawater under-saturation  $(1 - \Omega)$  (Fig. 2a). In situ aragonite dissolution experiments conducted during our cruise in the North Pacific have a temperature range of  $2\sim7$  °C, with an average value of 4.8 °C. Depths at which the experiments were conducted vary from 100 m to 2000 m (Table S2). Phosphate concentration varies from 0.06 to 3.24 µmol/kg. Lab experiments conducted with Dickson seawater have a constant phosphate concentration of 0.43 µmol/kg. Despite the discrepancies in the experimental conditions, in situ dissolution rates generally lie on the same curve, with a reaction order n of 1.37  $\pm$  0.18 over the  $\Omega$ range of 0.45 to 0.87 (Fig. 2b). Lab dissolution rates in acidified Dickson standard seawater at 5 °C show good agreement with field rates, while lab rates at 21 °C are two times faster than at 5°C. The reaction orders of lab dissolution rate laws at 5°C and 21 °C are 1.33  $\pm$  0.56 and 1.59  $\pm$  0.12 respectively. Between  $\Omega =$  $0.9\sim1$ , the reaction order n is smaller, indicated by a shallower slope in the log (dissolution rate) vs. log  $(1 - \Omega)$  plot (Fig. 2b). The  $\Omega_{critical}$  between the two rate law formulations is around 0.9  $(\log(1 - \Omega_{critical}) = -1.0).$ 

## 3.2. Sinking C fluxes captured by sediment traps

Mass export fluxes in the upper 200 m are higher in the North Pacific subarctic gyre than in the subtropical gyre by a factor of  $2\sim6$  (Fig. 3a-d). Total mass fluxes at 100 m in the subtropical gyre are approximately  $100\sim200~{\rm mg\,m^{-2}\,day^{-1}}$ , and increase sharply to  $\sim\!600~{\rm mg\,m^{-2}\,day^{-1}}$  at the transition zone. Total C fluxes account for 11~23% of total fluxes in the upper 200 m of the transect. PIC fluxes at 100 m vary from  $0.1 \sim 0.7$  mmol m<sup>-2</sup> day<sup>-1</sup> in the subtropical gyre, to  $1.0\sim2.5~\text{mmol}\,\text{m}^{-2}\,\text{day}^{-1}$  in the subarctic gyre; while at 200 m, PIC fluxes in the subarctic gyre are approximately 0.8 mmol m<sup>-2</sup> day<sup>-1</sup> (Table 1). Sinking PIC/POC molar ratios vary from 0.2 to 0.6, with no specific trend versus latitude. Total mass and C fluxes are higher at 100 m than 200 m by about a factor of 2 (Fig. 3e-h) although the attenuation with depth is much greater at higher latitude. Though all stations are supersaturated with respect to calcite between 100 and 200 m. and only Station 5 attains aragonite under-saturation above 200 m, a factor of 1.5~3 decrease in sinking PIC fluxes is observed at Station 2, 4

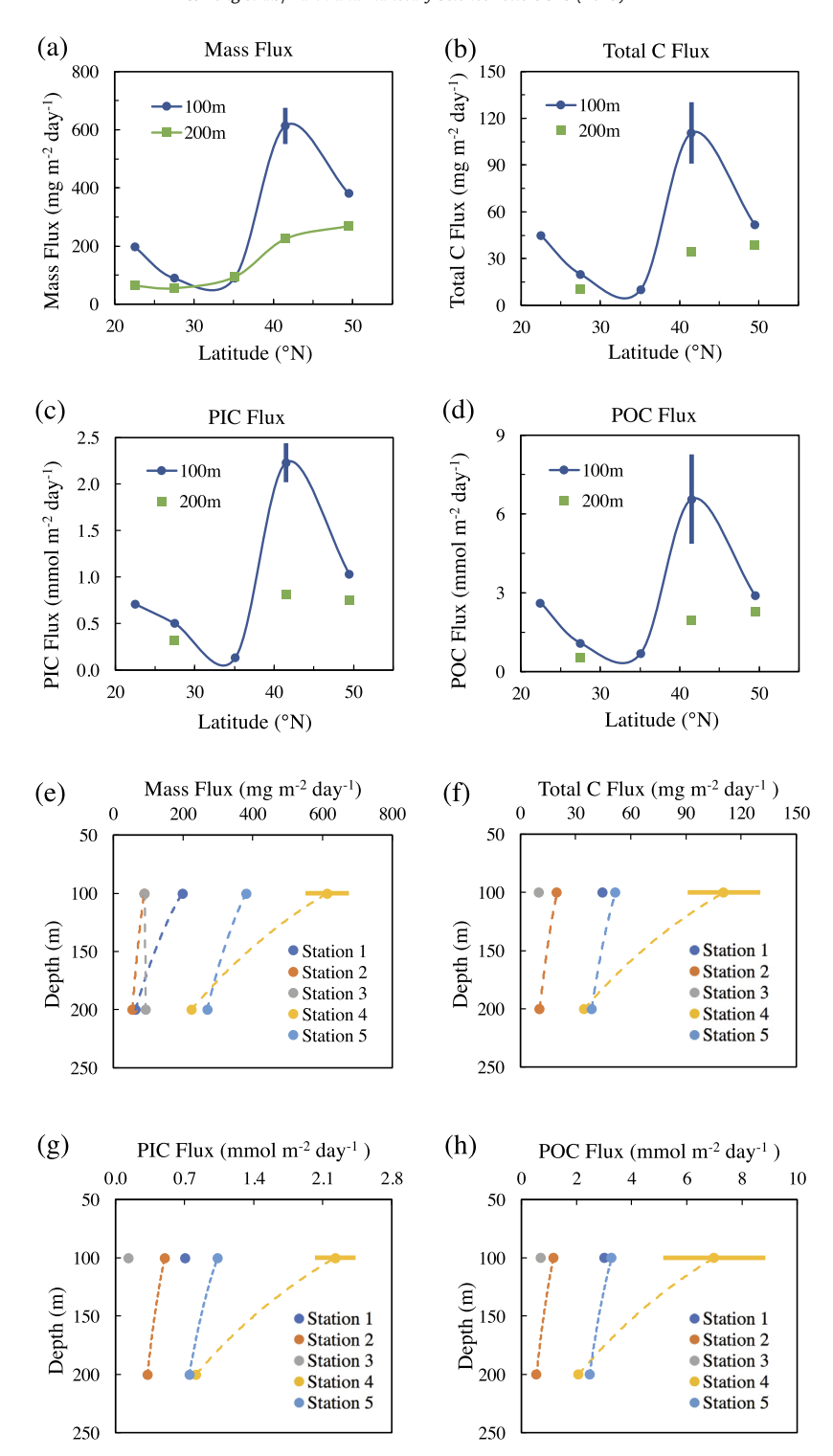


**Fig. 3.** Sinking fluxes captured by sediment traps at 100 m and 200 m along the North Pacific transect in August 2017. Station 1, 2, 3 were in the North Pacific subtropical gyre, while Station 4 and 5 were in the subarctic gyre. The solid bar for the 100 m sample at 42°N represent the difference in the duplicate samples at that site (the two ends of the bars are the duplicate values, and the trend lines are fitted through the average of the duplicates). (a–d) Fluxes vs. latitude; (e–h) fluxes vs. depth.

and 5 (Fig. 3g). Sample amounts were insufficient for C analysis at 200 m depth for Station 1 and 3.

Because Station 4 had abundant material in the trap tubes, only 3 tubes were combined from the 100 m trap whereas all other samples included material collected from 6 tubes. Therefore, a replicate analysis of flux values was determined for the 100 m trap at Station 4, demonstrating the variability in tube-to-tube collection efficiency and composition. The reproducibility of

mass, total C, PIC and POC flux is approximately 20%, 36%, 18% and 52% respectively.

In terms of mineral composition in the sediment traps, significantly higher percentages of calcite are observed in the subarctic gyre (Fig. 4a, 4b, Table 1). At both 100 m and 200 m in the subtropical gyre, calcite accounts for  $20\sim60\%$  of total CaCO<sub>3</sub>. However, in the subarctic gyre, the calcite percentage of total CaCO<sub>3</sub> exceeds 80% and constitutes the dominant sinking CaCO<sub>3</sub> phase. As a consequence, the apparent higher sinking flux observed in the

**Table 1** PIC fluxes, carbonate percentages and PIC/POC in sediment trap samples of CDisK-IV (August, 2017).

Station	Latitude	Longitude	Depth (m)	Total C flux (mg m <sup>-2</sup> day <sup>-1</sup> )	CaCO <sub>3</sub> flux (mmol m <sup>-2</sup> day <sup>-1</sup> )	Aragonite/CaCO <sub>3</sub>	PIC/POC
Station 1	22°45′N	157°59′W	100	44.8	0.71	44%	0.27
			200	N.A.	N.A.	67%	N.A.
Station 2	27°45′N	155°15′W	100	20.0	0.50	75%	0.46
			200	10.5	0.32	74%	0.60
Station 3	35°16′N	150°59′W	100	10.2	0.13	50%	0.19
			200	N.A.	N.A.	46%	N.A.
Station 4	41°45′N	148°16′W	100	$110.7 \pm 19.7$	$2.23 \pm 0.21$	10%	$0.34 \pm 0.09$
			200	34.8	0.82	14%	0.42
Station 5	49°50′N	149°39′W	100	51.7	1.03	9%	0.36
			200	38.7	0.75	8%	0.33

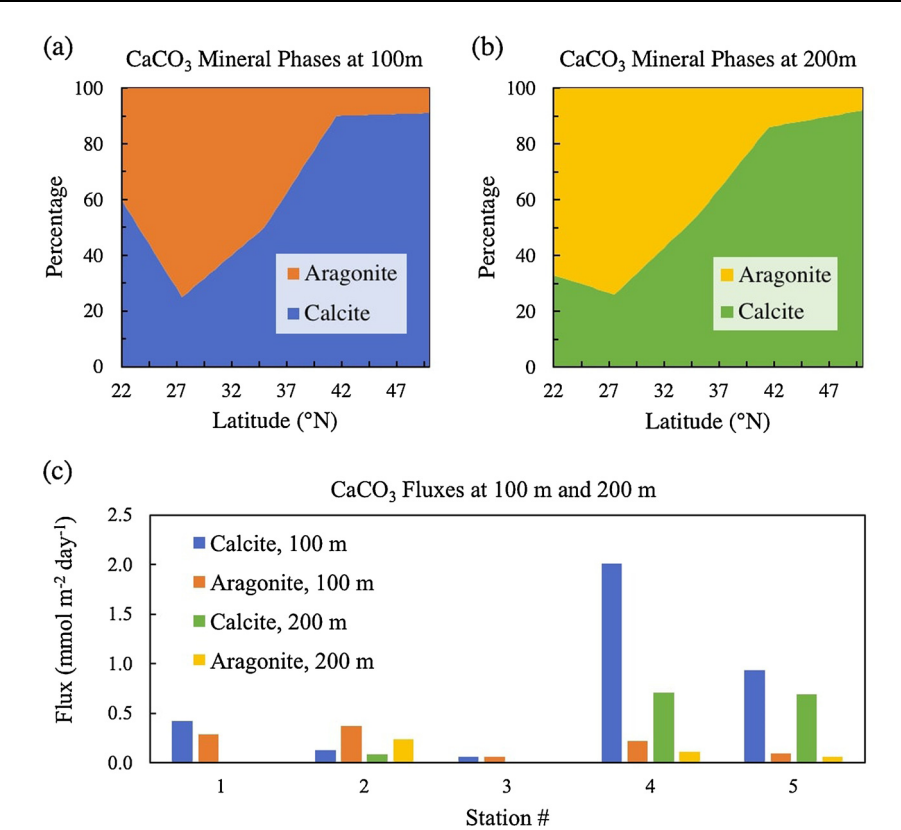


Fig. 4. CaCO3 mineral composition (a, b) and calculated mineral fluxes (c) in the sinking material along the North Pacific transect at 100 m and 200 m in August 2017.

subarctic gyre is mainly due to a significantly higher calcite flux, while the aragonite flux remains similar along the whole transect (Fig. 4c).

# 3.3. Suspended particulate C concentrations measured with in situ pumps

Suspended PIC and POC show quite different distribution patterns from each other along the North Pacific transect (Fig. 5a, 5b), resulting in a PIC/POC ratio that varies by a factor of  $8\sim10$ . A high concentration pool of suspended PIC ( $30\sim100~\mu m$ ) is detected in the upper 800 m centered at Station 3 ( $\sim35^\circ N$ ). In contrast, suspended POC at this latitude does not show high concentration at mid depth but simply decreases with depth as it does at all other stations. The PIC pool as measured on filter sub-samples agrees with observations of a concentrated suspended calcite pool detected by Raman scanning (Fig. 5c). The 'bullseye' of high PIC around Station 3 is supported by the Raman measurements and identified as suspended calcite. Throughout the water column, sus-

pended calcite concentrations are higher than aragonite concentrations by a factor of  $5{\sim}100$  (Fig. 5c, 5d). Aragonite particles are detected below 3000 m in the subtropical gyre (Fig. 5e). These aragonite particles include relatively large fragments (up to 190  $\mu m$ ) compared to calcite particles (<80  $\mu m$ ), indicating that large pteropod fragments are able to sink to the bottom of the ocean in the subtropical gyre. The average error of calcite or aragonite percentage in total PIC is 26% based on the three replicate filters analyzed (Table S3).

#### 4. Discussion

## 4.1. Kinetics of aragonite dissolution in the lab versus in the field

In previous studies, reported dissolution rate laws for aragonite as suspended particles in seawater were nonlinear, but the reaction order n varied (n=2.93 in Morse et al. (1979); n=4.2 in Keir (1980); n=1.87 in Acker et al. (1987)). In this study, we found  $n=1.4\pm0.2$  at 5 °C (lab and field) and  $1.6\pm0.1$  at 21 °C (lab) for

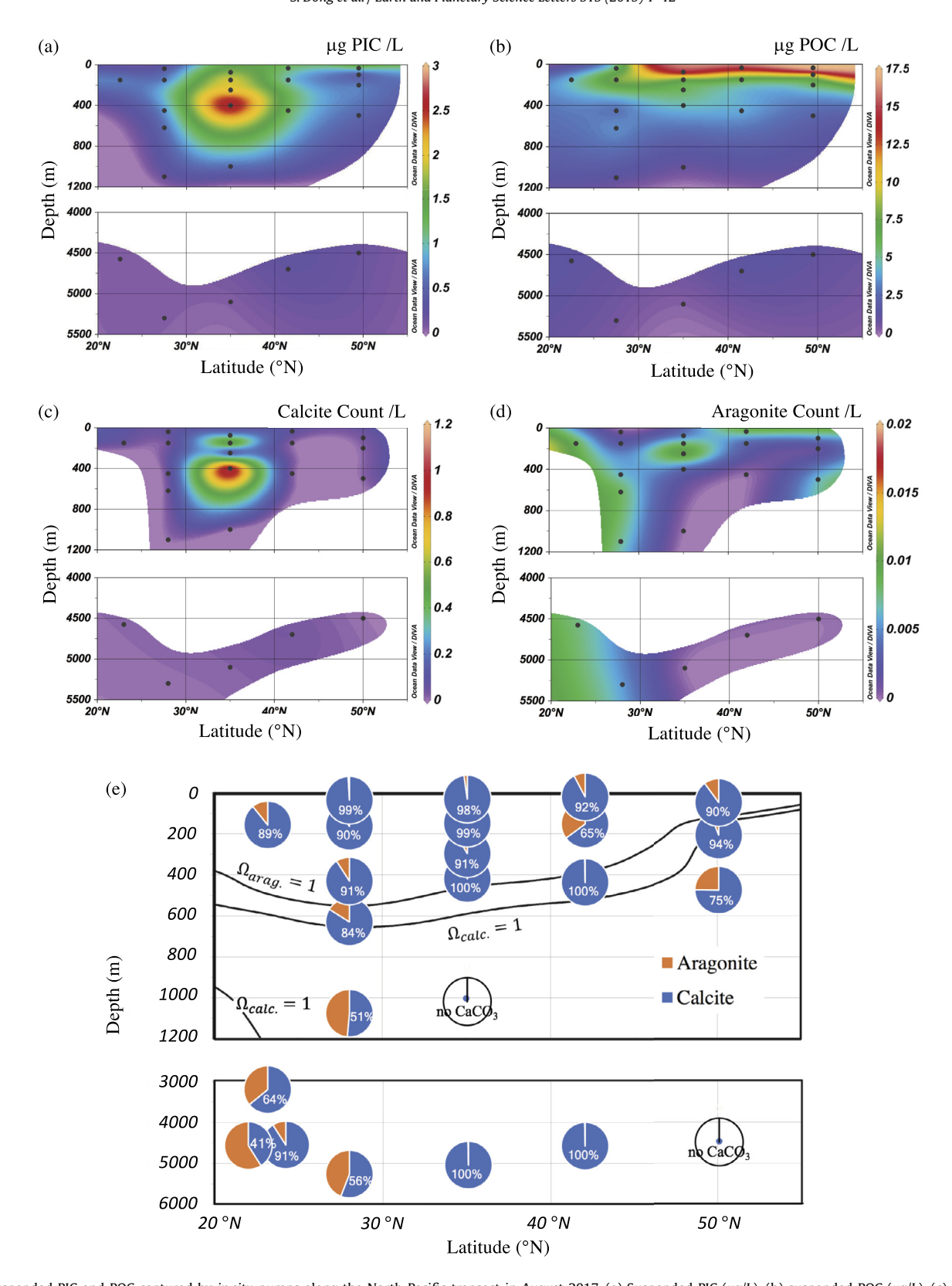


Fig. 5. Suspended PIC and POC captured by  $in \ situ$  pumps along the North Pacific transect in August 2017. (a) Suspended PIC ( $\mu g/L$ ), (b) suspended POC ( $\mu g/L$ ), (c) suspended calcite concentration (count/L), (d) suspended aragonite concentration (count/L), (e) calcite and aragonite percentages.

synthetic aragonite. A summary of dissolution rate data for aragonite in seawater (Fig. 6) calls for distinctions between lab studies vs. field studies, and experiments with synthetic aragonite vs. pteropods. First, dissolution rates measured *in situ* in the ocean water column are orders of magnitude slower than rates measured in

the lab. Second, whether the dissolution rates of synthetic aragonite agree with rates for pteropods appears to be dependent of the intrinsic crystal properties of the synthetic aragonite. In two lab dissolution studies, rates for synthetic aragonite were  $\sim\!30$  times faster than pteropod rates when normalized to surface area (Morse

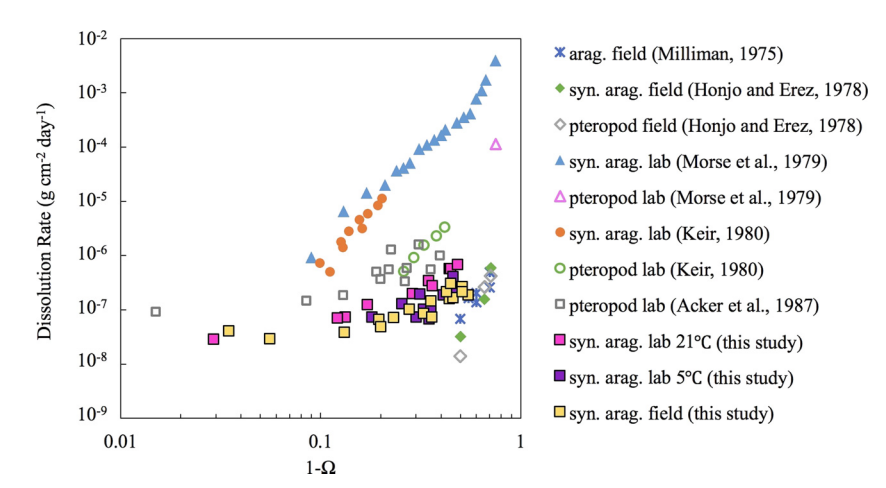


Fig. 6. Comparison of the aragonite dissolution rates in this study and previous studies. Closed symbols are dissolution rates of synthetic aragonite, whereas open symbols are rates of pteropods. Note that dissolution rates of synthetic aragonite are  $\sim$ 30 times larger than pteropods in Morse et al. (1979) and Keir (1980). Additionally, previously published field dissolution rates are orders of magnitude lower than lab dissolution rates. Dissolution rates reported in this study show a consistency between field and lab.

 Table 2

 Experimental conditions and materials used in published aragonite dissolution studies.

Material	Experimental condition	$\begin{array}{c} \text{SSA} \\ (\text{m}^2\text{g}^{-1}) \end{array}$	BET flow gas	Reference
Aragonite	Field	N.A.	N.A.	Milliman (1975)
Synthetic aragonite	Field	1.53	He	Honjo and Erez (1978)
Pteropds	Field	2.17	He	Honjo and Erez (1978)
Synthetic aragonite	Lab	1.4	Kr	Morse et al. (1979)
Pteropods	Lab	1.6	Kr	Morse et al. (1979)
Synthetic aragonite	Lab	1.4	Kr	Keir (1980)
Pteropods	Lab	2.17	He	Keir (1980)
Pteropods	Lab	N.A.	N.A.	Acker et al. (1987)
Synthetic aragonite	Lab and field	2.46	Kr	This study

<sup>\*</sup> SSA (specific surface area) not measured in Acker et al. (1987), specific rates ( $g \, cm^{-2} \, day^{-1}$ ) calculated assuming the same pteropods SSA as in Honjo and Erez (1978) and Keir (1980). Synthetic aragonite used in Morse et al. (1979) and Keir (1980), pteropod assemblage used in Honjo and Erez (1978) and Keir (1980) were samples of the same batch

et al., 1979; Keir, 1980). However, in a field dissolution study using a different synthetic aragonite, dissolution rates of synthetic aragonite and pteropods were in agreement (Honjo and Erez, 1978). The collection of all rates obtained from the literature and our work show a convergence of dissolution rate (surface area normalized) when  $\Omega>0.9.$  However, at lower saturation states, rates diverge by as much as 4 orders of magnitude.

This study is, as far as we know, the first to show consistency between lab and field CaCO<sub>3</sub> dissolution rates. It is also the first to use the exact same material in both environments. The field data agree with lab measurements conducted at 5 °C, whereas lab measurements at 21 °C are  $\sim\!\!2$  times faster for equivalent saturation state. While this temperature effect is not a central focus of our discussion, we note that it is similar to observations of the influence of temperature on calcite dissolution (Naviaux et al., 2019). An  $\Omega_{critical}$  at  $\sim\!\!0.9$  is observed for aragonite dissolution rates, similar to the value of  $\Omega_{critical}$  (0.87  $\pm$  0.05) between step retreat dissolution and defect-assisted dissolution for calcite dissolution recently reported in Dong et al. (2018), and  $\Omega_{critical}$  ( $\sim\!\!0.85$ ) for coccolith and foraminiferal biogenic calcite reported in Subhas et al. (2018).

The synthetic aragonite in this study dissolves significantly slower than the synthetic aragonites used by Morse et al. (1979) and Keir (1980). This could be due to lower defect density resulting from slower crystallization rates during our synthesizing process. The gel-diffusion methodology in this study allowed long crystal growth time, up to 3–6 months, whereas the precipitation time for the method of aragonite formation used by Morse et al. (1979) and Keir (1980) was  $\sim$ 30 min. Furthermore, the specific surface area

of the synthetic aragonite produced in this study  $(2.46 \text{ m}^2 \text{ g}^{-1})$  is similar to that of pteropods  $(2.17 \text{ m}^2 \text{ g}^{-1})$ , Honjo and Erez, 1978) (Table 2). We thus propose that the synthetic aragonite in this study is more representative of the pteropod aragonite. Our rates lie between the published dissolution rates of pteropods measured in the lab and in the field (Milliman, 1975; Honjo and Erez, 1978; Morse et al., 1979; Keir, 1980; Acker et al., 1987).

4.2. Total C and PIC export production rates, PIC/POC ratios in sinking fluxes and suspended materials in the North Pacific

Measured total C fluxes in the upper 200 m in the N. Pacific subtropical and subarctic gyre are  $0.85-3.73~\mathrm{mmol\,m^{-2}\,day^{-1}}$ ,  $2.90-9.23~\mathrm{mmol\,m^{-2}\,day^{-1}}$ , respectively (Table 1); comparable to the annual rate of net community production in the N. Pacific mixed layer reported by Lee (2001) (1.4–4.1  $\mathrm{mmol\,m^{-2}\,day^{-1}}$  in the subtropical gyre,  $5.5-8.2~\mathrm{mmol\,m^{-2}\,day^{-1}}$  in the subarctic gyre). PIC fluxes in the upper 200 m in the two gyres are  $0.13-0.71~\mathrm{mmol\,m^{-2}\,day^{-1}}$ ,  $0.75-2.23~\mathrm{mmol\,m^{-2}\,day^{-1}}$ ; slightly lower than the annual rate of net CaCO<sub>3</sub> production in Lee (2001) (0–1.6  $\mathrm{mmol\,m^{-2}\,day^{-1}}$  in the subtropical gyre,  $1.6-4.4~\mathrm{mmol\,m^{-2}\,day^{-1}}$  in the subarctic gyre).

PIC/POC molar ratios in sinking particles vary from  $0.19\sim0.60$  at 100 m and 200 m along the N. Pacific transect (Table 1), with no apparent trend with latitude. This range is inclusive of values measured with shallow sediment traps in the N. Pacific, including Station P (PIC/POC = 0.54 at 200 m), the Equatorial Pacific (PIC/POC = 0.1–0.5 at 125–340 m), and the W. Pacific Warm Pool (PIC/POC = 0.2–0.5 at 105–320 m) (Wong

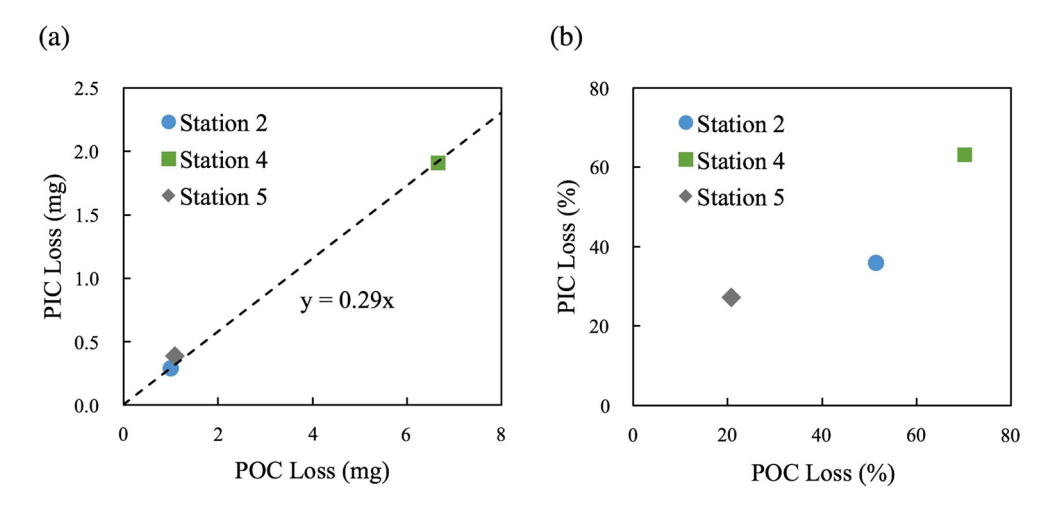


Fig. 7. Amount of PIC dissolved and POC remineralized between 100 m and 200 m in the sinking fluxes during CDisK-IV (August, 2017). (a) PIC weight loss as a function of POC weight loss, PIC dissolves and POC remineralizes at a ratio of 0.29. (b) Percent of PIC and POC lost from 100 m to 200 m. High PIC dissolution is associated with high POC remineralization.

et al., 1999; Rodier and Le Borgne, 1997; Honjo et al., 2008 and references therein). It is higher, however, than the estimated global mean rain ratio of 0.056 obtained by applying the vertical gradients of potential alkalinity and nitrate to an ocean biogeochemical-transport box model (Sarmiento et al., 2002 and references therein).

PIC/POC ratios in suspended particles cover a wider range than in sinking particles, varying from 0.06 to 0.81. Suspended particle concentrations measured by in situ pumps are considered to represent a semi-decomposed phase generated from sinking particles but also from particles embedded in an advecting water mass. The high concentration of suspended PIC observed in the upper 800 m between 30 and 40°N is confirmed by PIC analysis via filter acidification (Fig. 5a) and by calcite grain counts via Raman scanning (Fig. 5c). One explanation for this high PIC concentration pool is potentially the not-yet-dissolved carbonate produced during the previous weeks to months when the transition zone resided near that latitude. The absence of high aragonite concentrations within this pool could be due to a) lack of production or b) the lower saturation state of aragonite at this depth than calcite, and thus more rapid dissolution. Further to the north, where there is high PIC export, seawater is under-saturated at shallower depth and the suspended PIC is much lower. The fact that there is no bullseye pattern observed in suspended POC indicates that POC associated with this PIC has a much shorter residence time in the upper ocean. This agrees with the finding of higher PIC/POC ratios in deeper sediment traps reported in Berelson et al. (2007). One consequence of POC remineralization is that it can leave PIC unprotected and exposed to seawater for dissolution. Although this bullseve is distinct, dissolution of the suspended PIC in this pool will generate a maximum excess alkalinity of only 0.3 µmol/kg, which is trivially small. However, this bullseye pattern is potentially a tracer of dissolution of a larger sinking PIC flux. It is the transformation from the flux of particulate sinking carbonate to suspended carbonate, and subsequently to dissolved carbonate that helps define the ocean alkalinity balance.

The presence of suspended aragonite particles below 3000 m in the subtropical gyre (Fig. 5e) provides direct evidence that aragonite aggregates can sink towards the bottom of the ocean without being fully dissolved. Because the sediments at these depths have PIC <0.1 wt.%, benthic dissolution of aragonite should therefore be considered when constructing carbon cycle simulations.

4.3. PIC dissolution and POC remineralization rates in sinking fluxes and shallow depth dissolution

The following discussion of trap flux data is predicated on our assumption that trapping with PIT traps is accurate and equally efficient at 100 m and 200 m. Work with these identical traps (Haskell et al., 2013) exhibited good agreement between Th-based POC flux and sediment-trap-based POC flux, although the traps occasionally yielded fluxes smaller than those obtained via Th methodologies. Another confirmation that our traps are representative of the true export in this region is a comparison of the fluxes we obtained at Station 1 and work by others at Station Aloha. The floating PITs trap results of Karl and Church (2014) yielded an average POC flux of 2.5 mmol m<sup>-2</sup> day<sup>-1</sup> at 150 m, comparable to our 100 m trap flux of 2.6 mmol m<sup>-2</sup> day<sup>-1</sup>.

The difference in sediment trap PIC fluxes between 100 m and 200 m at the same location indicates that a large fraction of the sinking PIC dissolves in this zone (27 $\sim$ 63%, Fig. 3g). This occurs at one site that is under-saturated with respect to aragonite between 100 m and 200 m (e.g., Station 5;  $\Omega = 1.3 \sim 0.5$ ), but also at stations super-saturated at this depth (Station 2 and 4;  $\Omega = 3 \sim 2.7$ and  $\Omega = 1.8 \sim 1.5$  respectively). This analysis is in direct conflict with determinations of calcium carbonate dissolution rates (Fig. 2), which show no appreciable dissolution when  $\Omega > 1$ . Although supported by only a few data, a strong correlation between PIC dissolution and POC remineralization rates is observed (Fig. 7), with a molar ratio of 0.29 at all three stations (Fig. 7a). Higher percentages of POC loss are associated with higher percentages of PIC loss, with 20 $\sim$ 70% POC loss between 100 m and 200 m, and 30 $\sim$ 60% PIC loss (Fig. 7b). The similar calcite to aragonite ratios at 100 m and 200 m (Fig. 4a, 4b) indicates that calcite and aragonite dissolve at similar ratios relative to their abundance. Therefore, dissolution mechanism for the shallow depth dissolution is not sensitive to carbonate mineral phase, and has less direct dependence on saturation state.

It has been suggested that organic matter respiration can produce microenvironments with locally enhanced CO<sub>2</sub> concentration, and therefore promote dissolution well above the saturation horizon (Jansen et al., 2002). Aerobic respiration has been shown to decrease oxygen concentrations within sinking aggregates (Ploug, 2001). We propose that respiration-driven dissolution is one potential mechanism underlying the observed attenuation of sinking PIC fluxes observed in this study. Another possible reason is that both POC and PIC are consumed by large organisms (metazoans) or zooplankton. PIC is dissolved during gut

passage (Bishop et al., 1980; Harris, 1994). The percentage of PIC and POC loss may have temporal variation because microbial and metazoan/zooplankton abundances may vary seasonally. At Station 5, where seawater is under-saturated for aragonite below 100 m, thermodynamically-driven dissolution may also occur and contribute alongside respiration-driven dissolution, and/or metazoan/zooplankton consumption to the observed attenuation.

# 4.4. Calcite/aragonite ratios in sinking and suspended materials in the North Pacific water column

Previous studies of aragonite and calcite sinking fluxes were determined using traps and defined mineral species by microscopic identification (Betzer et al., 1984; Fabry and Deuser, 1991) and Xray diffraction analysis (Berner and Honjo, 1981; Fabry and Deuser, 1991). Betzer et al. (1984) reported a  $0.3 \, \text{mmol} \, \text{m}^{-2} \, \text{day}^{-1}$  average flux of aragonite at 100 m, compared to 0.057 mmol  $m^{-2}$  day<sup>-1</sup> at 400 m and 0.009 mmol  $m^{-2}$  day<sup>-1</sup> at 2200 m along a Northwestern Pacific section, yielding a 90% loss in the upper 2200 m. Their absolute flux rates showed that foraminifera were more abundant in the northern areas (aragonite/total  $CaCO_3 = 9 \sim 33\%$  north of 42°N) whereas pteropods dominated in the southern areas (aragonite/total CaCO<sub>3</sub> =  $66 \sim 95\%$  south of  $30^{\circ}$ N). A rather constant aragonite flux through depth was reported in the Sargasso Sea, with aragonite accounting for 8~35% of total CaCO<sub>3</sub> (Fabry and Deuser, 1991). Their average pteropod mass flux from 7 trap deployments were  $0.026 \pm 0.006 \text{ mmol m}^{-2} \, \text{day}^{-1}$  at 500 m,  $0.024 \pm 0.004$  ${\rm mmol}\,{\rm m}^{-2}\,{\rm day}^{-1}$  at 1500 m, and 0.024  $\pm$  0.002 mmol  ${\rm m}^{-2}\,{\rm day}^{-1}$ at 3200 m. Similar values were reported at the Panama Basin  $(\sim 0.06 \text{ mmol m}^{-2} \text{ day}^{-1} \text{ at } 667 \text{ m to } \sim 0.03 \text{ mmol m}^{-2} \text{ day}^{-1} \text{ at}$ 3791 m) and the Equatorial Atlantic (0.168 mmol  $m^{-2}$  day<sup>-1</sup> at 389 m to 0.034 mmol  $m^{-2}$  day<sup>-1</sup> at 988 m), with aragonite accounting for 4~39% of total CaCO<sub>3</sub> (Berner and Honjo, 1981).

In this study, lower aragonite/calcite ratios are observed in sediment trap materials in the subarctic gyre (aragonite <20%) than in the subtropical gyre (aragonite 37~75%) (Fig. 4a, 4b). This distribution pattern is similar to the Northwestern Pacific section in Betzer et al. (1984). The increase in PIC and POC fluxes across the transition zone (from south to north) is mainly due to an increase in calcite species, and the aragonite fluxes remain similar along the whole transect (Fig. 4c). The aragonite fluxes we determined; 0.07 to 0.38 mmol m $^{-2}$  day $^{-1}$  at 100 m, and 0.06 to 0.24 mmol m $^{-2}$  day $^{-1}$  at 200 m, are comparable to the average aragonite flux at 100 m (0.3 mmol m $^{-2}$  day $^{-1}$ ) in Betzer et al. (1984). The higher calcite percentage north of the transition zone also agrees with the conclusion of Juranek et al. (2012), wherein the authors related the increased Transition Zone Chlorophyll Front productivity to a high amount of coccolithophorids and diatoms.

## 4.5. Aragonite dissolution fluxes in the North Pacific water column

According to the dissolution experiments in Byrne et al. (1984), abundant small size class aragonite particulates were suggested to provide substantial contributions to the "excess alkalinity" of the upper water column of the Pacific Ocean. However, Fabry (1990) estimated the pteropod and heteropod growth rate to yield 0.029 mmol  $\text{CaCO}_3 \text{ m}^{-2} \text{ day}^{-1}$ , only sufficient to account for  $\sim 8\%$  of the calculated rate of  $\text{CaCO}_3$  dissolution in the North Pacific, were this to completely dissolve upon sinking. Similar to aragonite, high-Mg calcite has also been suggested to account for the shallow dissolution phenomenon due to its high solubility. Carbonate formed within fish, a Mg-rich calcite, was reported to explain up to a quarter of the increase in titratable alkalinity within 1000 m of the ocean surface (Wilson et al., 2009).

In the North Pacific, maximum *in situ* dissolution rates of approximately 1.1  $\mu$ mol kg<sup>-1</sup> yr<sup>-1</sup> were reported at 530 m by plot-

ting excess alkalinity (TA\*) versus water parcel ages derived from chlorofluorocarbon-11 (CFC-11) (Feely et al., 2004). This high dissolution rate at shallow depths was associated with either dissolution in locally acidic conditions, including guts of zooplankton (Bishop et al., 1980; Harris, 1994), and where bacterial oxidation of organic matter takes place (Jansen and Wolf-Gladrow, 2001); or dissolution of the more soluble forms of CaCO3 in shallow waters, including pteropods and high-Mg calcite (Byrne et al., 1984). Recent studies also pointed out the significance of the enzyme carbonic anhydrase in enhancing carbonate dissolution rates in the ocean (Subhas et al., 2017) and the kinetic enhancement of CaCO<sub>3</sub> dissolution rates due to pressure (Dong et al., 2018). The calculation below assesses whether the inorganic dissolution of sinking aragonite alone can account for the excess alkalinity observed (Fig. 8a, 8b), and how much of the dissolution can be driven by organic matter respiration and metazoan/zooplankton grazing (Fig. 8c, 8d).

We construct a box model of the water column to diagnose the sinking and dissolution of  $CaCO_3$  particles in the upper 2000 m. Particles are considered to be produced in the upper 100 m within the euphotic zone, and are exposed to dissolution while sinking. PIC, calcite and aragonite fluxes at the bottom of the euphotic zone, saturation states in the water column, and dissolution rates are based on the measurements in this study. A three orders of magnitude difference in aragonite sinking rate (0.1 m/day to 100 m/day) is adopted to investigate the effect of sinking rates on aragonite dissolution fluxes. First, to estimate the dissolution flux due to inorganic aragonite dissolution, sinking aragonite particles are considered to be exposed to dissolution when the water column first reaches  $\Omega < 1$ , and dissolution rates are determined as a function of  $\Omega$  according to the relationship shown in Fig. 2. Details of the model can be found in supplementary materials.

Model results show that the sinking rate of aragonite aggregates significantly alters the sinking flux vs. depth and in situ dissolution signals (Fig. 8a, 8b). To generate the observed in situ CaCO3 dissolution rates (0.8 $\sim$ 1.2 µmol kg<sup>-1</sup> yr<sup>-1</sup> between 250 and 750 m) in the water column as reported in Feely et al. (2004), the sinking rate of aragonite flux will have to be much less than  $1 \text{ m day}^{-1}$ . This sinking rate is lower than generally accepted pteropod sinking rates of  $80\sim1080~{\rm m\,day^{-1}}$  (Noji et al., 1998). Assuming a pteropod sinking rate of 100 m day<sup>-1</sup>, our measured aragonite sinking flux and dissolution rate only account for 0.2% of the excess alkalinity signal. The implication of this model result is that the thermodynamically-driven dissolution of sinking aragonite particles alone is inadequate to explain the excess alkalinity observed in the North Pacific water column, and that other mechanisms, e.g. respiration-driven dissolution and/or metazoan/zooplankton consumption, are required to explain the shallow depth dissolution.

The mechanism for both respiration-driven dissolution and metazoan/zooplankton consumption is that acidic local microenvironment is provided and drives PIC dissolution. As a result, CaCO $_3$  dissolution can take place above the saturation horizon. To approximate this type of dissolution, a model is developed in which sinking fluxes at 100 m are taken from measurements using sediment traps, and a constant dissolution rate of 40% every 100 m is assumed based on the calculated dissolution rate between 100 and 200 m (Fig. 7b). PIC, calcite and aragonite sinking fluxes at 100 m ( $Flux_{100m}$ ) are 1.2 mmol m $^{-2}$  day $^{-1}$ , 0.8 mmol m $^{-2}$  day $^{-1}$ , and 0.4 mmol m $^{-2}$  day $^{-1}$ , respectively.

Model results show that the *in situ* dissolution signal produced by either respiration-driven dissolution or metazoan/zooplankton consumption in the upper 600 m is significantly higher than thermodynamically-driven dissolution fluxes (Fig. 8c, 8d), and is comparable in magnitude to the observed dissolution signal reported in Feely et al. (2004). However, the shape of the modeled *in situ* dissolution rate appears to be different than the observed

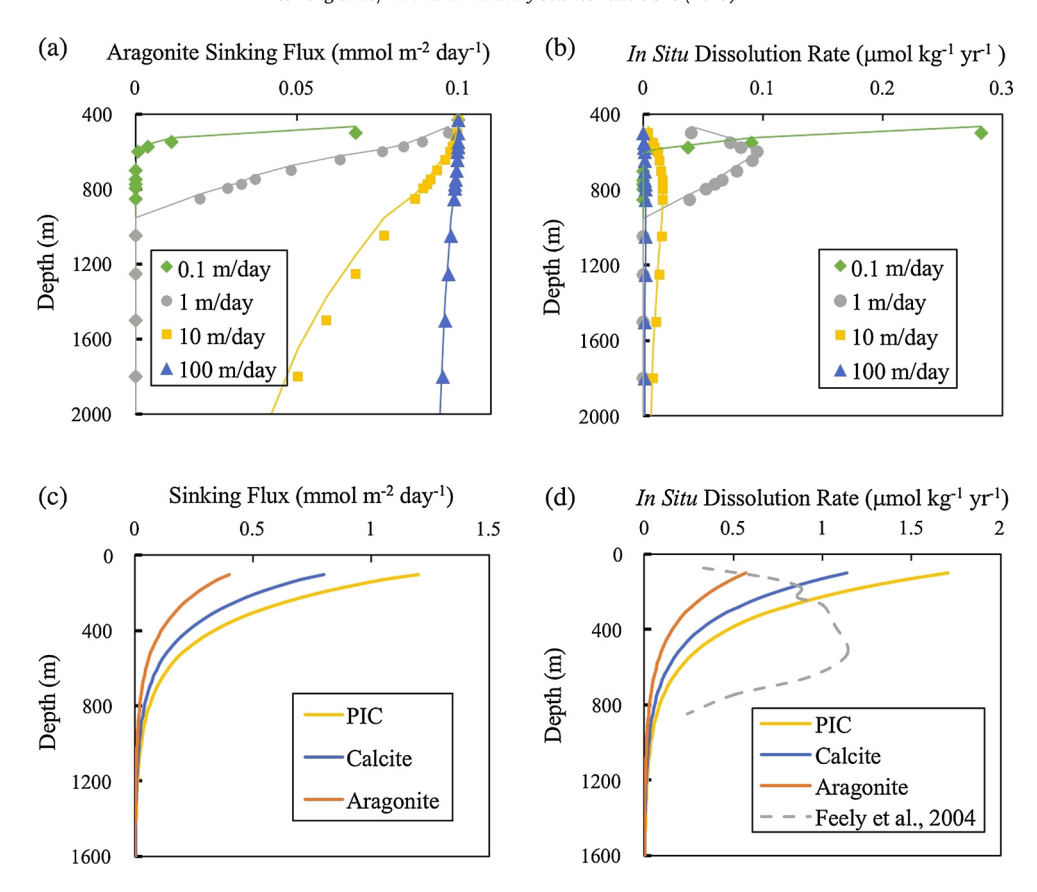


**Fig. 8.** (a) Aragonite sinking flux below the saturation horizon (430 m) if dissolution only occurs as abiotic aragonite dissolution; (b) *in situ* dissolution rate in the water column (µmol  $kg^{-1}yr^{-1}$ ) if dissolution only occurs as abiotic aragonite dissolution. Different symbols in (a) and (b) represent different sinking rates of aragonite particles. Dissolution rates are calculated based on the saturation states measured in Station 3 (35°N, 151°W) and the dissolution rate law determined in this paper. Aragonite sinking flux of 0.1 mmol m<sup>-2</sup> day<sup>-1</sup> is assumed to reach 430 m, below which seawater starts to become under-saturated. (c) PIC sinking flux assuming 40% dissolution every 100 m due to organic matter respiration driven dissolution or metazoan/zooplankton consumption; (d) *in situ* dissolution rate generated by respiration driven dissolution or metazoan/zooplankton consumption. For (c), (d), total PIC sinking flux of 1.2 mmol m<sup>-2</sup> day<sup>-1</sup>, calcite flux of 0.8 mmol m<sup>-2</sup> day<sup>-1</sup>, aragonite flux of 0.4 mmol m<sup>-2</sup> day<sup>-1</sup> assumed at 100 m.

pattern. This could be due to vertical mixing in the mixing layer, horizontal transport, and/or the re-utilization of alkalinity in the surface by shell-making biota. The magnitude of shallow depth dissolution may be sensitive to seasonality because microbial and metazoan/zooplankton abundances may vary seasonally.

# 5. Conclusions

We report dissolution rates of synthetic aragonite in seawater both in the lab (at 5 °C and 21 °C) and in the field ( $2\sim7$  °C) along a transect from Hawaii to Alaska, and show consistency between lab rates at 5 °C and field rates. Aragonite dissolution rates (at  $5^{\circ}$ C) fit a non-linear rate equation: Rate (g g<sup>-1</sup> day<sup>-1</sup>) = 0.013 \*  $(1-\Omega)^{1.37}$  . Rates are  $\sim 2$  times faster at 21 °C than at 5 °C for equivalent saturation state. As determined by floating sediment traps deployed on this transect, sinking carbon fluxes are significantly higher in the subarctic gyre than in the subtropical gyre, and yet there is no geographical trend in PIC/POC mole ratio, which is 0.2~0.6 for material sinking between 100 and 200 m. The calcite/aragonite ratio is lower in the subtropical gyre than in the subarctic gyre. Calcite fluxes in the two gyres are different by a factor of  $5\sim10$ , whereas aragonite fluxes appear relatively constant along the North Pacific transect. Measured aragonite fluxes are 0.07~0.38  ${\rm mmol}\,{\rm m}^{-2}\,{\rm day}^{-1}$  at 100 m, and  $0.06{\sim}0.24~{\rm mmol}\,{\rm m}^{-2}\,{\rm day}^{-1}$  at 200 m, with no specific trend over latitude. A comparison of fluxes at depths 100 m to 200 m indicates that 30~60% PIC dissolves between these depths with a simultaneous 20~70% attenuation in POC fluxes. The presence of suspended aragonite below 3000 m in the subtropical gyre indicates that large pteropod fragments can sink to the bottom of the ocean without being fully dissolved. One significant implication of this study is that predictions based on a strictly thermodynamic view of aragonite dissolution underestimate observed alkalinity excess and measured PIC attenuation. This conclusion is indicated by the unreasonably low sinking rate of pteropod aragonite ( $<1~{\rm m\,day^{-1}}$ ) required to generate the excess alkalinity described in Feely et al. (2004). Our measured aragonite flux and inorganic dissolution rate only account for 9% and 0.2% of the excess alkalinity observed in the North Pacific, assuming a pteropod sinking rate of 1 m day<sup>-1</sup> and 100 m day<sup>-1</sup>, respectively. Respiration-driven dissolution or metazoan/zooplankton grazing, indicated by the simultaneous attenuation of PIC and POC in the sediment traps versus depth, produces an amount of dissolution comparable to that suggested by excess alkalinity but not consistent with the depth distribution.

# Acknowledgements

This work was supported by NSF Ocean Acidification grants (numbers OCE1220600 and OCE1220302), USC Dornsife Doctoral Fellowship, Elizabeth and Jerol Sonosky Fellowship, the Sea Grant Fellowship, and the Resnick Sustainability Institute Graduate Fellowship. The authors would like to acknowledge editor Derek Vance, reviewer Jack Middelburg and another anonymous reviewer for their invaluable comments of the original manuscript. We thank the captain and crews on Kilo Moana for their assistance at sea. We also acknowledge Christopher Moore, Loraine Martell-Bonet for their help measuring pH and alkalinity during CDisK-IV; Yi Hou for leak-checking the Niskin Incubators by measuring dis-

solved Si concentrations; Doug Hammond for providing the *in situ* pumps; Johnny Stutsman and James Rae for their help deploying and recovering *in situ* pumps; as well as Abby Lunstrum and Huanting Hu for their help picking out swimmers from the sediment trap samples.

## Appendix A. Supplementary material

Supplementary material related to this article can be found online at https://doi.org/10.1016/j.epsl.2019.03.016.

#### References

- Acker, J.G., Byrne, R.H., Ben-Yaakov, S., Feely, R.A., Betzer, P.R., 1987. The effect of pressure on aragonite dissolution rates in seawater. Geochim. Cosmochim. Acta 51, 2171–2175.
- Anderson, L.A., Sarmiento, J.L., 1994. Redfield ratios of remineralization determined by nutrient data analysis. Glob. Biogeochem. Cycles 8, 65–80.
- Balch, W.M., Gordon, H.R., Bowler, B.C., Drapeau, D.T., Booth, E.S., 2005. Calcium carbonate measurements in the surface global ocean based on Moderate-Resolution Imaging Spectroradiometer data. J. Geophys. Res., Oceans 110 (C7).
- Berelson, W.M., 2001. Particle settling rates increase with depth in the ocean. Deep Sea Res. Part 2, Top. Stud. Oceanogr. 49 (1–3), 237–251.
- Berelson, W.M., Balch, W.M., Najjar, R., Feely, R.A., Sabine, C., Lee, K., 2007. Relating estimates of CaCO<sub>3</sub> production, export, and dissolution in the water column to measurements of CaCO<sub>3</sub> rain into sediment traps and dissolution on the sea floor: a revised global carbonate budget. Glob. Biogeochem. Cycles 21 (1).
- Berger, W.H., 1978. Deep-sea carbonate: pteropod distribution and the aragonite compensation depth. Deep-Sea Res. 25 (5), 447–452.
- Berner, R.A., Honjo, S., 1981. Pelagic sedimentation of aragonite: its geochemical significance. Science 211 (4485), 940–942.
- Betzer, P.R., Byrne, R.H., Acker, J.G., Lewis, C.S., Jolley, R.R., Feely, R.A., 1984. The oceanic carbonate system: a reassessment of biogenic controls. Science 226 (4678), 1074–1077.
- Bishop, J.K., Wood, T.J., 2008. Particulate matter chemistry and dynamics in the twilight zone at VERTIGO ALOHA and K2 sites. Deep-Sea Res., Part 1, Oceanogr. Res. Pap. 55 (12), 1684–1706.
- Bishop, J.K., Collier, R.W., Kettens, D.R., Edmond, J.M., 1980. The chemistry, biology, and vertical flux of particulate matter from the upper 1500 m of the Panama Basin. Deep-Sea Res., A, Oceanogr. Res. Pap. 27 (8), 615–640.
- Boyd, P.W., Trull, T.W., 2007. Understanding the export of biogenic particles in oceanic waters: is there consensus? Prog. Oceanogr. 72 (4), 276–312.
- Byrne, R.H., Acker, J.G., Betzer, P.R., Feely, R.A., Cates, M.H., 1984. Water column dissolution of aragonite in the Pacific Ocean. Nature 312, 321–326.
- Dong, S., Subhas, A.V., Rollins, N.E., Naviaux, J.D., Adkins, J.F., Berelson, W.M., 2018. A kinetic pressure effect on calcite dissolution in seawater. Geochim. Cosmochim. Acta 238, 411–423.
- Fabry, V.J., 1989. Aragonite production by pteropod molluscs in the subarctic Pacific. Deep-Sea Res., A, Oceanogr. Res. Pap. 36 (11), 1735–1751.
- Fabry, V.J., 1990. Shell growth rates of pteropod and heteropod molluscs and aragonite production in the open ocean: implications for the marine carbonate system. J. Mar. Res. 48 (1), 209–222.
- Fabry, V.J., Deuser, W.G., 1991. Aragonite and magnesian calcite fluxes to the deep Sargasso Sea. Deep-Sea Res., A, Oceanogr. Res. Pap. 38 (6), 713–728.
- Feely, R.A., Sabine, C.L., Lee, K., Berelson, W., Kleypas, J., Fabry, V.J., Millero, F.J., 2004. Impact of anthropogenic CO<sub>2</sub> on the CaCO<sub>3</sub> system in the oceans. Science 305 (5682), 362–366.
- Gangstø, R., Gehlen, M., Schneider, B., Bopp, L., Aumont, O., Joos, F., 2008. Modeling the marine aragonite cycle: changes under rising carbon dioxide and its role in shallow water CaCO<sub>3</sub> dissolution. Biogeosciences 5 (4), 1057–1072.
- Gehlen, M., Bassinot, F.C., Chou, L., McCorkle, D., 2005. Reassessing the dissolution of marine carbonates: II. Reaction kinetics. Deep-Sea Res., Part 1, Oceanogr. Res. Pap. 52 (8), 1461–1476.
- Harris, R.P., 1994. Zooplankton grazing on the coccolithophore Emiliania huxleyi and its role in inorganic carbon flux. Mar. Biol. 119 (3), 431–439.
- Haskell II, W.Z., Berelson, W.M., Hammond, D.E., Capone, D.G., 2013. Particle sinking dynamics and POC fluxes in the Eastern Tropical South Pacific based on <sup>234</sup>Th budgets and sediment trap deployments. Deep Sea Res. Part 1, Oceanogr. Res. Pap. 81, 1–13.
- Hong, G.H., Chen, C.T.A., 2002. Aragonitic pteropod flux to the interior of the East Sea (Sea of Japan). Terr. Atmos. Ocean. Sci. 13 (2), 205–210.
- Honjo, S., Erez, J., 1978. Dissolution rates of calcium carbonate in the deep ocean; an in-situ experiment in the North Atlantic Ocean. Earth Planet. Sci. Lett. 40 (2), 287–300.

- Honjo, S., Manganini, S.J., Cole, J.J., 1982. Sedimentation of biogenic matter in the deep ocean. Deep-Sea Res., A, Oceanogr. Res. Pap. 29 (5), 609–625.
- Honjo, S., Manganini, S.J., Krishfield, R.A., Francois, R., 2008. Particulate organic carbon fluxes to the ocean interior and factors controlling the biological pump: a synthesis of global sediment trap programs since 1983. Prog. Oceanogr. 76 (3), 217–285
- Iglesias-Rodriguez, M.D., Armstrong, R., Feely, R., Hood, R., Kleypas, J., Milliman, J.D., Sabine, C., Sarmiento, J., 2002. Progress made in study of ocean's calcium carbonate budget. Eos Trans. AGU 83 (34), 365–375.
- Jansen, H., Wolf-Gladrow, D.A., 2001. Carbonate dissolution in copepod guts: a numerical model. Mar. Ecol. Prog. Ser. 221, 199–207.
- Jansen, H., Zeebe, R.E., Wolf-Gladrow, D.A., 2002. Modeling the dissolution of settling CaCO<sub>3</sub> in the ocean. Glob. Biogeochem. Cycles 16 (2), 11.
- Juranek, L.W., Quay, P.D., Feely, R.A., Lockwood, D., Karl, D.M., Church, M.J., 2012. Biological production in the NE Pacific and its influence on air-sea CO<sub>2</sub> flux: evidence from dissolved oxygen isotopes and O<sub>2</sub>/Ar. J. Geophys. Res., Oceans 117 (C5).
- Karl, D.M., Church, M.J., 2014. Microbial oceanography and the Hawaii Ocean timeseries programme. Nat. Rev. Microbiol. 12 (10), 699.
- Keir, R.S., 1980. The dissolution kinetics of biogenic calcium carbonates in seawater. Geochim. Cosmochim. Acta 44 (2), 241–252.
- Klaas, C., Archer, D.E., 2002. Association of sinking organic matter with various types of mineral ballast in the deep sea: implications for the rain ratio. Glob. Biogeochem. Cycles 16 (4).
- Lee, K., 2001. Global net community production estimated from the annual cycle of surface water total dissolved inorganic carbon. Limnol. Oceanogr. 46 (6), 1287–1297.
- Lohmann, G.P., 1995. A model for variation in the chemistry of planktonic foraminifera due to secondary calcification and selective dissolution. Paleoceanography 10, 445–457.
- Milliman, J.D., 1975. Dissolution of aragonite, Mg-calcite, and calcite in the North Atlantic Ocean. Geology 3 (8), 461–462.
- Mohan, R., Verma, K., Mergulhao, L.P., Sinha, D.K., Shanvas, S., Guptha, M.V.S., 2006. Seasonal variation of pteropods from the Western Arabian Sea sediment trap. Geo Mar. Lett. 26 (5), 265–273.
- Morse, J.W., de Kanel, J.O.H.N., Harris, K.A.R.E.N., 1979. Dissolution kinetics of calcium carbonate in seawater; VII, The dissolution kinetics of synthetic aragonite and pteropod tests. Am. J. Sci. 279 (5), 488–502.
- Mucci, A., 1983. The solubility of calcite and aragonite in seawater at various salinities, temperatures, and one atmosphere total pressure. Am. J. Sci. 283 (7), 780–709
- Naviaux, J.D., Subhas, A.V., Rollins, N.E., Dong, S., Berelson, W.M., Adkins, J.F., 2019. Temperature dependence of calcite dissolution kinetics in seawater. Geochim. Cosmochim. Acta 246, 363–384.
- Nickl, H.J., Henisch, H.K., 1969. Growth of calcite crystals in gels. J. Electrochem. Soc. 116 (9), 1258–1260.
- Noji, T.T., Bathmann, U.V., Von Bodungen, B., 1998. Clearance of picoplankton-sized particles and formation of rapidly sinking aggregates by the pteropod, Limacina retroversa. Oceanogr. Lit. Rev. 1 (45), 107.
- Ploug, H., 2001. Small-scale oxygen fluxes and remineralization in sinking aggregates. Limnol. Oceanogr. 46 (7), 1624–1631.
- Rodier, M., Le Borgne, R., 1997. Export flux of particles at the equator in the western and central Pacific ocean. Deep-Sea Res., Part 2, Top. Stud. Oceanogr. 44 (9–10), 2085–2113.
- Sarmiento, J.L., Dunne, J., Gnanadesikan, A., Key, R.M., Matsumoto, K., Slater, R., 2002.

  A new estimate of the CaCO<sub>3</sub> to organic carbon export ratio. Glob. Biogeochem. Cycles 16 (4).
- Schiebel, R., 2002. Planktonic foraminiferal sedimentation and the marine calcite budget. Glob. Biogeochem. Cycles 16, 1065. https://doi.org/10.1029/2001GB001459.
- Subhas, A.V., Adkins, J.F., Rollins, N.E., Naviaux, J., Erez, J., Berelson, W.M., 2017. Catalysis and chemical mechanisms of calcite dissolution in seawater. Proc. Natl. Acad. Sci. USA 114 (31), 8175–8180.
- Subhas, A.V., Rollins, N.E., Berelson, W.M., Dong, S., Erez, J., Adkins, J.F., 2015. A novel determination of calcite dissolution kinetics in seawater. Geochim. Cosmochim. Acta 170, 51–68.
- Subhas, A.V., Rollins, N.E., Berelson, W.M., Erez, J., Ziveri, P., Langer, G., Adkins, J.F., 2018. The dissolution behavior of biogenic calcites in seawater and a possible role for magnesium and organic carbon. Mar. Chem. 205, 100–112.
- Wilson, R.W., Millero, F.J., Taylor, J.R., Walsh, P.J., Christensen, V., Jennings, S., Grosell, M., 2009. Contribution of fish to the marine inorganic carbon cycle. Science 323 (5912), 359–362.
- Wong, C.S., Whitney, F.A., Crawford, D.W., Iseki, K., Matear, R.J., Johnson, W.K., Page, J.S., Timothy, D., 1999. Seasonal and interannual variability in particle fluxes of carbon, nitrogen and silicon from time series of sediment traps at Ocean Station P, 1982–1993: relationship to changes in subarctic primary productivity. Deep-Sea Res., Part 2, Top. Stud. Oceanogr. 46 (11–12), 2735–2760.